Interdependency of optical constants in *a*-C and *a*-C:H thin films interpreted in light of the density of electronic states

G. Fanchini and A. Tagliaferro
Dipartimento di Fisica & Unità INFM, Politecnico di Torino, Torino, Italy

D. P. Dowling, K. Donnelly, M. L. McConnell, R. Flood, and G. Lang
Surface Engineering Group, Enterprise Ireland, Glasnevin, Dublin 9, Ireland
(Received 26 March 1999; revised manuscript received 1 November 1999)

The real and imaginary parts of the dielectric constants for several *a*-C(:H) thin films were measured in the energy range 1.5–4.5 eV. The data were analyzed assuming Gaussian shapes for the ''valence'' and ''conduction'' π bands and scaling the energy by means of the Gaussian width parameter σ. At any given scaled energy Y an approximately linear relationship was obtained between the real and the imaginary part of dielectric constant. The energy dependence of the slope and intercept of such lines are analytically determined on the basis of the quoted Gaussian-shaped density of states. The existence of a Cauchy behavior for the contribution to the real part of the dielectric constant due to the transitions other than π-π^* is shown. The role of disorder in determining the necessity for a scaled energy based analysis was addressed.

INTRODUCTION

Amorphous carbon thin films have been proposed for a number of applications involving the protection of optical devices against wear.[1] A detailed knowledge of the optical properties of such films is therefore crucially important. The optical constants of *a*-C(:H) coatings are however determined by the density of electronic states which, in turn, are influenced by the type and nature of bonds between ions and by the microstructure. For this reason knowledge of the optical constants can represent a useful tool to improve the knowledge about the density of states and the microstructure of *a*-C(:H) coatings.

A key point to be remembered in the analysis of the optical constants of *a*-C(:H) films is that a considerable number of sp^2 sites is always present.[2] The π states pertaining to such sites show a low energy spacing between bonding and antibonding states, so that they sit nearer Fermi level than the σ states (arising either from the sp^2 or the sp^3 sites). As a consequence, the optical transitions for photon energies in the visible and near ultraviolet energy range ($E = 1.5$–4.5 eV) essentially occur through π-electron excitation by incident radiation. The sp^3 sites (mainly characterized by σ states) give a weak contribution, arising from the σ-band tails. The method of determining the optical constants once the density of states is given, is quite straightforward and is described in several textbooks.[3] It is clear that the energy dependence of the optical constants is related to the shape of the density of states. One should then expect the wide variety of sp^3/sp^2 ratios and hydrogen contents to lead to very different energy dependencies of the optical constants. As demonstrated in Fig. 1, however, there appears to be a quasilinear relationship between *a*-C(:H) film refractive index (n) and extinction coefficient (k). These results are representative of optical measurements obtained for a very large number of *a*-C and *a*-C:H coatings, at the photon energy of $E = 1.84$ eV, irrespectively of the deposition method and of the hydrogen and sp^2 contents.[4,5]

The objective of this paper is to provide a theoretical basis for such experimental results. It will be shown that a theoretical relationship exists over the photon energy range 1.5–4.5 eV. This relationship will be demonstrated starting from a previously reported model of the optical properties of amorphous carbon films,[6] based on the assumption of Gaussian-shaped π and π^* bands. It will be shown that a linear correlation exists between the real (ε_1) and imaginary (ε_2) parts of the dielectric constants and, as a consequence and with a certain degree of approximation, between the refractive index n and the extinction coefficient k. It will also be shown that a quantitative agreement among the experimental and the theoretical values of the intercept and the slope of such lines at all considered energies can be obtained if the role of disorder is properly taken into account.

EXPERIMENT

The *a*-C films were deposited using a saddle field source onto 75×25 mm^2 soda glass substrates from pure acetylene. The glass substrates were argon bombarded prior to deposition. The source operated at 1000 V and a pressure of $1 - 9 \times 10^{-3}$ mbar. Increasing the deposition pressure at a given source power decreased the refractive index of the deposited film and enabled a range of films to be deposited. With respect to hydrogen content, it has been previously reported[7] that the hydrogen content of saddle beam deposited films has been measured using both secondary ion mass spectrometry (SIMS) and thermal desorption techniques. The latter measurement involved heating the coated samples in vacuum up to 520 °C; effused hydrogen was then measured using a mass spectrometer. Only adsorbed hydrogen was detected on the films, no hydrogen was detected in the bulk of the film.

The *a*-C:H films were deposited in a 25 liter stainless steel chamber again on soda glass substrates, placed onto a 10-cm diameter driven electrode. Deposition was achieved at

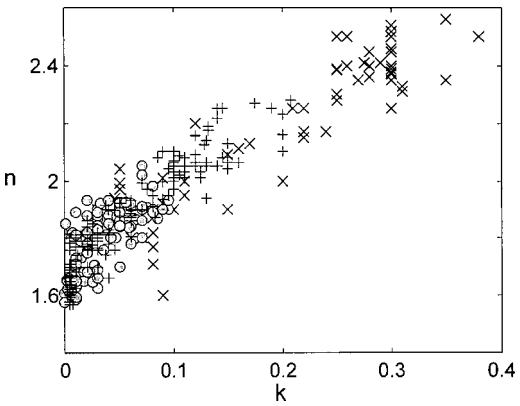

FIG. 1. A plot of refractive index vs extinction coefficient (at a photon energy $E = 1.84$ eV) of several *a*-C(:H) films as determined using *in situ* ellipsometry. Films include those deposited from 13.56 MHz RF plasmas (○), 40 kHz pulsed dc plasmas (+), and from the saddle field atom source (×).

either 40 kHz or 13.56 MHz from C_2H_2, He, Ar, and H_2 as detailed in previous papers.[4,5] Again a range of films was obtained by changing the deposition pressure.

In situ ellipsometry (at $\lambda = 675$ nm) was used to measure the refractive index, extinction coefficient, and thickness of the coatings. A list of the *a*-C(:H) coatings on which this study is based is given in Table I along with *n* and *k* values obtained at $\lambda = 675$ nm. The coatings were also examined using spectral ellipsometry. The measurements were performed at room temperature to evaluate the film thickness and refractive index. The measurements were carried out using a Jobin Yvon UVISEL variable angle spectral ellipsometer in the energy range 1.5 to 4.5 eV (wavelength 827 to 275 nm) and good agreement was obtained with the *in situ* measurements.

EXPERIMENTAL RESULTS

Though all films reported in Table I (in order of increasing optical gap values) have been considered in the following analysis, in order to avoid a loss of clarity, in Figs. 2(a) and 2(b) we have plotted the energy dependence of the refractive index (*n*) and the extinction coefficient (*k*) for four representative samples having very different optical and physical properties. For instance, film *C*7 is characterized by a lower concentration of π states than film *C*1, as shown by the lower *k*-values for *C*7. Moreover, we can see that the maximum *k* values of samples *C*7 and *C*1 are different by a factor of 2.3, while the shapes of the two curves are not dissimilar. The energy dependence of the refractive index is quite different among the quoted samples and is even at odd in sample *C*1 (which will be dealt with later). The differences, however, are more apparent than real, as shown in Fig. 3(a) (where the optical constants are plotted as *n* vs *k*) and in Fig. 3(b) (where the optical constants are plotted as ε_1 vs ε_2). It is now clear that, despite the scale differences, related to the different density of sp^2 sites, the differences in the energy dependences are due to the fact that we are examining different parts of the energy spectrum of the optical constants for each sample.

Since the goal is to explain the experimental relationship found in Refs. 4 and 5, a linear interpolation of the *n* vs *k* data has been performed on the nine films for each of the 0.05 eV spaced energy values in the range 1.5–4.5 eV. A typical result (regarding the behavior at $E = 2.2$ eV) is reported in Fig. 4(a). As quoted in the Introduction, the physically meaningful relationship we are looking for is that between the two parts of the dielectric constant. For this reason we have shown in Fig. 4(b) the ε_1 vs ε_2 relationship at the same energy.

TABLE I. *a*-C(:H) coatings considered in the present work.

Coating Label	Coating Type	Deposition Method [a]	n [b]	k [b]	Thickness [nm]
*C*1	*a*-C	SF	2.48	0.27	200
*C*2	*a*-C	SF	2.09	0.15	200
*C*3	*a*-C:H	RF	2.01	0.08	200
*C*4	*a*-C	SF	1.99	0.06	260
*C*5	*a*-C:H	MW	1.98	0.07	120
*C*6	*a*-C:H	RF	1.84	0.02	270
*C*7	*a*-C:H	RF	1.93	0.02	230
*C*8	*a*-C	SF	1.89	0.01	195
*C*9	*a*-C:H	MW	1.83	0.02	120

[a] RF = 13.56 MHz plasma. SF = saddle field plasma. MW = 40 kHz plasma.
[b] $E = 1.84$ eV.

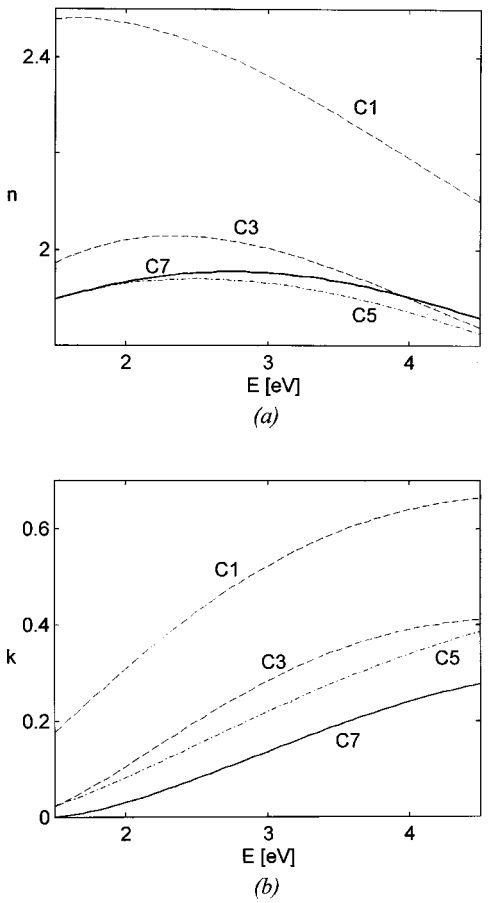

FIG. 2. Energy dependence of the refractive index *n* (a) and of the extinction coefficient *k* (b) for samples *C*1, *C*3, *C*5, and *C*7.

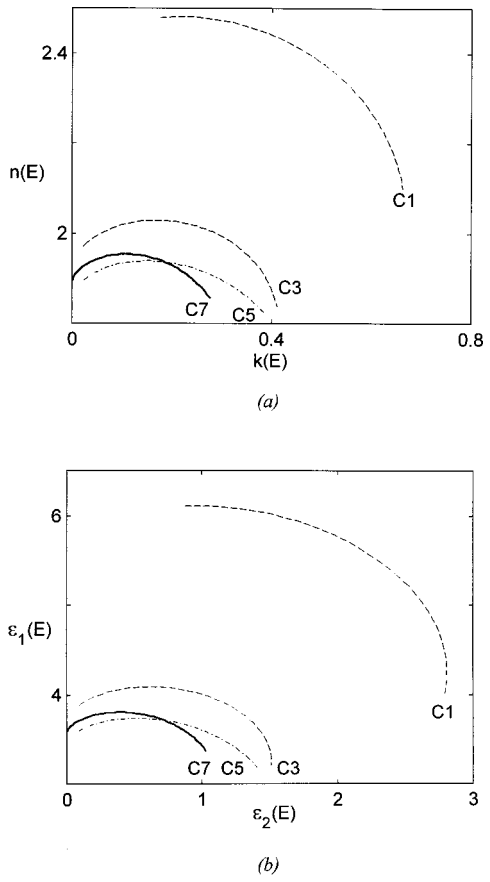

FIG. 3. (a) $n(E)$ vs $k(E)$. (b) Real $[\varepsilon_1(E)]$ vs imaginary $[\varepsilon_2(E)]$ part of the dielectric constant plot for samples $C1$, $C3$, $C5$, and $C7$, in the energy range of Fig. 2. Energy increases as k and ε_2.

From each plot (i.e., at any given photon energy E) of the types reported in Fig. 4, it has been extracted the slopes of the $n(E)$ vs $k(E)$ [and $\varepsilon_1(E)$ vs $\varepsilon_2(E)$] interpolating lines as well as their intercepts with the y axis. Such values are plotted in Figs. 5(a) and 5(b), respectively. The task in the following sections will be to find an explanation for the trend versus energy and the actual values of such curves.

THEORY

It has been shown by several authors (see for instance Ref. 3) that the proper way to approach the response of a solid to an alternating electromagnetic field arises from the analysis of the complex dielectric constant

$$\varepsilon(E)=\varepsilon_1(E)+i\varepsilon_2(E). \tag{1}$$

The imaginary part ε_2 is the most directly related to the density of states and to the electronic properties in solids. However, as the interaction of radiation with matter is concerned, the following relations [the well-known Kramers-Krönig (KK) relationships] will hold between the two components of the dielectric constant, ε_1 and ε_2:

$$\varepsilon_1(E)=1+\frac{2}{\pi}\int_0^\infty \frac{E'\varepsilon_2(E')}{E'^2-E^2}dE' \tag{2a}$$

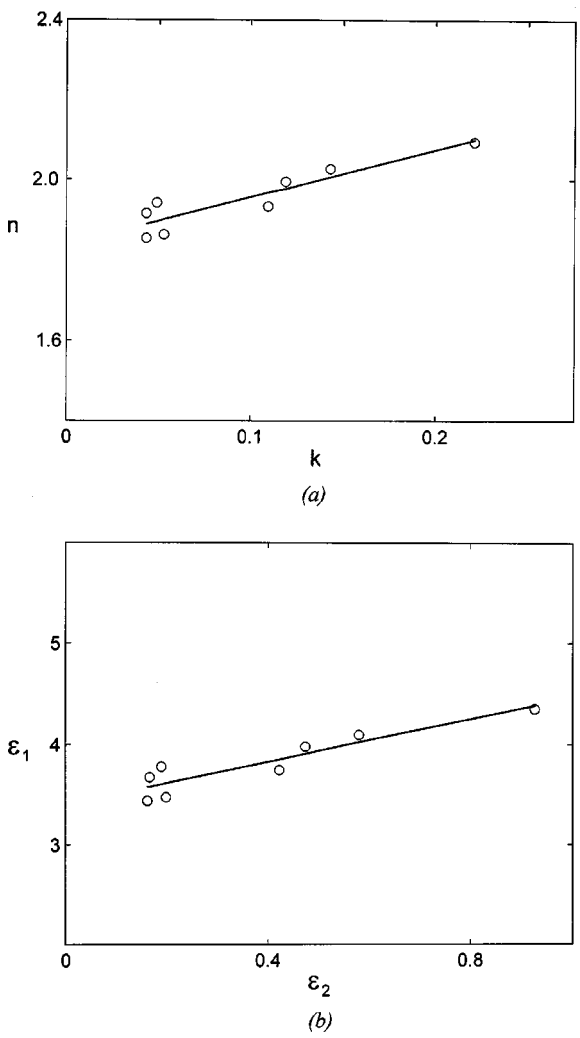

FIG. 4. Linear interpolation of (a) the n vs k and (b) the ε_1 vs ε_2 data for eight films at $E=2.2$ eV.

$$\varepsilon_2(E)=\frac{2}{\pi}E\int_0^\infty \frac{\varepsilon_1(E')}{E'^2-E^2}dE'. \tag{2b}$$

Such equations are in fact a general feature of causal systems, describing the detail of such interaction.[8] Moreover, complex refractive index and complex dielectric constant are immediately related, since

$$\varepsilon_1(E)=n^2(E)-k^2(E) \tag{3a}$$

$$\varepsilon_2(E)=2n(E)k(E). \tag{3b}$$

Relationships (2) and (3) suggest a way to approach the problem: at first, determine or assume (see below) an expression for ε_2, so that, by means of the KK Eq. (2a), the expression for ε_1 may be determined. Taking advantage of such a relation, the existence, at a given photon energy, of the linear relationship between ε_1 and ε_2 will be shown. Finally, using Eqs. (3a)–(3b), the n vs k function will be determined.

THE IMAGINARY PART OF DIELECTRIC CONSTANT

When each type j of optical transition gives its contributions, the overall imaginary part of the dielectric constant can be obtained by summing up such contributions:

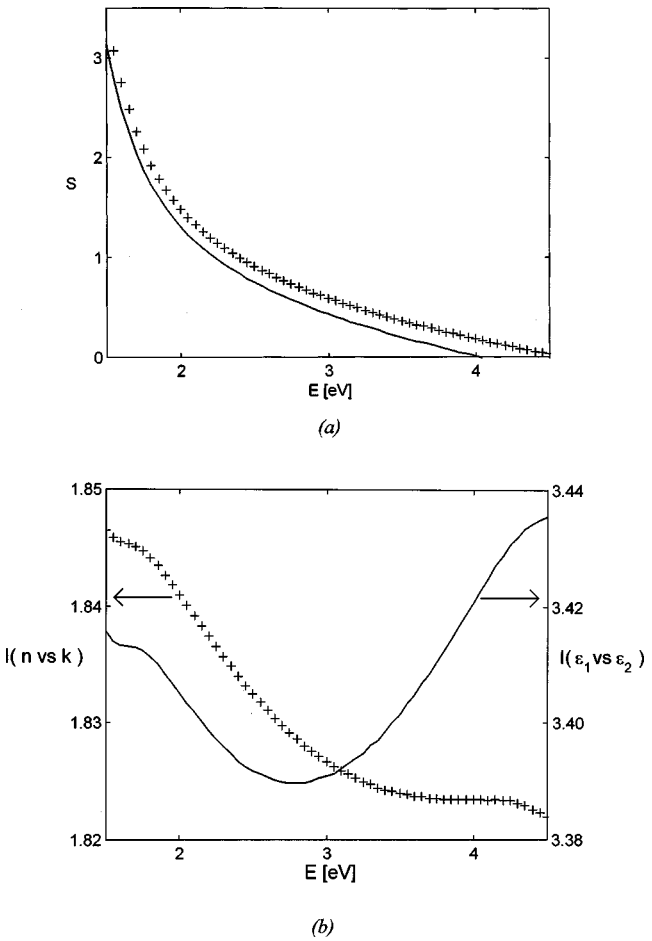

FIG. 5. Energy dependence (a) of the slopes (b) of the intercepts of the linear n vs k (++) and ε_1 vs ε_2 (—) interpolations. Note the similarity of values and trend for the slopes.

$$\varepsilon_2(E)=\sum_j \varepsilon_{2,j}(E). \tag{4a}$$

By replacing Eq. (4a) into Eq. (2a), it can be shown that

$$\varepsilon_1(E)-1=\frac{2}{\pi}\int_0^{\pi}\frac{E'\Sigma_j\varepsilon_{2j}(E')dE'}{E'^2-E^2}=\sum_j\,[\varepsilon_{1,j}(E)-1]. \tag{4b}$$

As the optical transitions of a-C(:H) thin films are concerned, it has to be considered[9] that the energy region of the density-of-states sitting 2–3 eV above and below Fermi level is made up mainly by π states. This means that in the energy region of interest in the present work ($E=1.5$–4.5 eV) we can assume that only π-π^* transitions give an appreciable contribution to excitation, therefore

$$\varepsilon_2(E)=\varepsilon_{2\sigma}(E)+\varepsilon_{2\pi}(E)\approx\varepsilon_{2\pi}(E), \tag{5a}$$

where $\varepsilon_{2\pi}(E)$ represents the contribution of π-π^* transitions, while, in the present paper, we'll indicate as $\varepsilon_{2\sigma}(E)$ the contribution of all other transitions (σ-π^*, σ-σ^*,$\cdots$). On the other hand, because of the peculiar form of Eq. (2a), all transitions will give their contribution to the susceptivity $\varepsilon_1(E)-1$ [and to the refractive index $n(E)$]. Therefore, from Eq. (4b), we can write

$$\varepsilon_1(E)=\varepsilon_{1\sigma}(E)+\varepsilon_{1\pi}(E)-1. \tag{5b}$$

In the following paragraphs, we will take advantage of Eqs. (5) in order to work out a quantitative explanation for the $\varepsilon_1(E)$ vs $\varepsilon_2(E)$ and $n(E)$ vs $k(E)$ relationships reported in Fig. 4.

Gaussian-DOS model

When only π-π^* transitions are considered, optical properties of amorphous carbon thin films (and, especially, the imaginary part of dielectric constant) can be modeled[6] as arising from Gaussian shaped π and π^* bands. The following expression for $\varepsilon_{2\pi}(E)$ can be obtained:[6]

$$\varepsilon_{2\pi}(E)=\frac{Q}{N_v n_\pi E^2}\int_{E_F}^{E_F+E}N_\pi(E'-E)N_\pi^*(E')dE'$$
$$=\frac{A}{E^2}\,\mathrm{erf}\left(\frac{E}{2\sigma_\pi}\right)\exp\left[-\left(\frac{E}{2\sigma_\pi}-\frac{2E_\pi}{2\sigma_\pi}\right)^2\right], \tag{6}$$

where N_v is the number of valence π electrons per atom.

N_π and N_π^* represent the Gaussian-shaped densities of bonding (π) and antibonding (π^*) states.

Q depends upon the dipole matrix element of the optical transitions. As previously shown[3] this is almost independent of energy, as far as the suitable matrix element is chosen. Actually, Q depends as well upon film density, but this dependence will not be considered here.

$2E_\pi$ is the interband peak-to-peak energy, while E_π is the distance of each Gaussian with respect to the Fermi level, E_F.

σ_π is the Gaussian width related to the local disorder in sp^2 sites.

The magnitude of each of valence and conduction Gaussian bands is proportional to the concentration n_π of the π states (i.e., of the sp^2 carbon sites) in the film, so that[6]

$$A=\frac{\sqrt{\pi}Q\sigma_\pi n_\pi}{N_v}. \tag{7}$$

With a different grouping of terms, we can rewrite Eq. (6) as

$$\varepsilon_{2\pi}(E)=\frac{n_\pi}{\sigma_\pi}f_G\left(Y_G=\frac{E}{2\sigma_\pi},W_G=\frac{2E_\pi}{2\sigma_\pi}\right), \tag{8}$$

where n_π depends on the sp^2 fraction and the film density only. It is worth noting that:

(1) the only first-order effect of a variation in the sp^2 concentration is to change the value of n_π.

(2) f_G depends on only two dimensionless variables (Y_G and W_G).

Gaussian-ν model

For reasons which will become hopefully clear later, we will now perform a slight modification of the just described Gaussian-density of states (DOS) model, based on the optical oscillator strength density

$$\nu(E)=\frac{m_e}{2\pi^2\hbar e^2}E\varepsilon_{2\pi}(E), \tag{9}$$

TABLE II. Optical gaps, Gaussian-DOS model (E_π and σ_π) and Gaussian-ν model (P_π and σ'_π) parameters.

Sample	*C*1	*C*2	*C*3	*C*4	*C*5	*C*6	*C*7	*C*8	*C*9
E_{04} [eV]	1.15[a]	1.48[a]	1.73	1.80	1.80	2.14	2.18	2.22	2.22
E_π [eV]	2.28	2.35	2.37	2.46	2.56	2.65	2.70	2.61	2.55
σ_π [eV]	1.02	1.07	0.94	1.00	0.99	0.92	0.93	0.87	0.80
P_π [eV]	4.00	4.13	4.15	4.32	4.50	4.64	4.73	4.58	4.48
σ'_π [eV]	1.04	1.09	0.96	1.02	1.01	0.93	0.94	0.88	0.81
W_ν	1.92	1.89	2.16	2.12	2.23	2.49	2.52	2.60	2.77

[a]Extrapolated.

where e and m_e are respectively the charge and rest mass of the electron. Although $\nu(E)$ was originally proposed to represent the number of electrons involved in optical transitions induced by photons having energy E, more sophisticated treatment has shown that its interpretation is somewhat more complicated.[8] However, it still remains that the integral over all energies of such quantity represents the total number per unit volume of electrons involved in the transitions. As π bands are concerned, this indicates that

$$n_\pi = \int_0^\infty \nu(E')dE' = \frac{m_e}{2\pi^2\hbar e^2}\int_0^\infty E'\varepsilon_{2\pi}(E')dE'. \quad (10)$$

In the framework of the Gaussian-DOS model described above, the $\nu(E)$ value is given by

$$\begin{aligned}\nu(E) &= \nu(Y_G, W_G)\\ &= \frac{m_e A}{2\pi^2\hbar e^2 E}\,\mathrm{erf}\left(\frac{E}{2\sigma_\pi}\right)\exp\left[-\left(\frac{E}{2\sigma_\pi}-\frac{2E_\pi}{2\sigma_\pi}\right)^2\right]\\ &= \frac{m_e n_\pi}{4\pi^2\hbar e^2 Y_G} f_G\left(Y_G=\frac{E}{2\sigma_\pi}, W_G=\frac{2E_\pi}{2\sigma_\pi}\right), \quad (11)\end{aligned}$$

where f_G is as defined in Eq. (8), but the disappearance of the additional factor $1/\sigma_\pi$ present in such equation has to be noticed. This avoids the loss of generality in the Gaussian-DOS model due to this factor, as Eq. (11) depends on n_π and dimensionless parameters (Y_G and W_G) only. However, our interest in $\nu(E)$ is mainly due to the fact that, in the present case, a Gaussian shaped oscillator strength $\nu(E)$, namely

$$\nu(E) = \frac{m_e}{2\pi^2\hbar e^2} B \exp\left[-\left(\frac{E-P_\pi}{2\sigma'_\pi}\right)^2\right], \quad (12)$$

is consistent with the assumption of Gaussian π-DOS, if the shape of factor erf(Y)/Y [see Eqs. (7) and (8)], is approximately Gaussian. The ν-model Gaussian parameters, P_π and σ'_π, will be roughly of the same order of $2E_\pi$ and σ_π (though $P_\pi < 2E_\pi$ and $\sigma'_\pi > \sigma_\pi$, see Table II for the actual values).

By replacing Eq. (12) in Eq. (10), B is shown to be proportional to the concentration, n_π, of π states in the film

$$B \propto n_\pi. \quad (13)$$

Such relationship will play, in the Gaussian-ν model, the role played by Eq. (7) in the Gaussian π-DOS model. The new model will allow as well a schematic expression for the imaginary part of dielectric constant of the form

$$\varepsilon_{2\pi}(E) = \frac{n_\pi}{\sigma'_\pi} f_\nu\left(Y_\nu=\frac{E}{2\sigma'_\pi}, W_\nu=\frac{P_\pi}{2\sigma'_\pi}\right), \quad (14)$$

where the function f_ν has the same form as the f_G function of Eq. (8). Note, however, that the Y_ν axis can be differently scaled in the two models, since $\sigma_\pi \neq \sigma'_\pi$.

The advantage of the present model is that it allows an analytical solution of $\varepsilon_1(E)$ vs $\varepsilon_2(E)$ and $n(E)$ vs $k(E)$ relationships, not achievable by the Gaussian-DOS model.

THE ε_1 VS ε_2 BEHAVIOR

Time has now come to address the main point of this paper: the $\varepsilon_1(E)$ vs $\varepsilon_2(E)$ behavior. By assuming excitation to be described by Eq. (5a) (i.e., $\varepsilon_2 \approx \varepsilon_{2\pi}$) in the energy region of interest, Eq. (5b) can be rewritten as

$$\varepsilon_1(E) \approx \varepsilon_{1\sigma}(E) + \frac{\varepsilon_{1\pi}(E)-1}{\varepsilon_{2\pi}(E)}\varepsilon_2(E). \quad (15)$$

Our interest, as shown in the last sections, is not focused onto the energy E, but on the scaled energies Y_G or Y_ν. Therefore let us rewrite Eq. (15) as

$$\varepsilon_1(Y_i) \approx \varepsilon_{1\sigma}(Y_i) + \frac{\varepsilon_{1\pi}(Y_i)-1}{\varepsilon_{2\pi}(Y_i)}\varepsilon_2(Y_i), \quad (15a)$$

which holds for both $i=G$ and $i=\nu$. The susceptivity to excitation ratio for π-π^* transitions in such equation can be evaluated by substituting Eq. (8) [or (11)] in the KK relationship [Eq. (2a)]:

$$\frac{\varepsilon_{1\pi}-1}{\varepsilon_{2\pi}} = \frac{\frac{2}{\pi}\int_0^\infty \frac{Y' f_i(Y', W_i)}{Y'^2 - Y_i^2}dY'}{f_i(Y_i, W_i)} = S(Y_i, W_i), \quad (16)$$

which still holds for both $i=G$ and $i=\nu$. The dependence of S on the sp^2 fraction (i.e., on deposition parameters, hydrogenation, etc.) is limited to a second-order effect, such as fluctuations in the values of the $W_G = E_\pi/\sigma_\pi$ [or $W_\nu = P_\pi/(2\sigma'_\pi)$] ratios. If W_G (or W_ν) is the same (or almost the same) for a set of samples, then Eq. (16) shows that a linear relationship between the measured values of $\varepsilon_1(Y_i)$ and $\varepsilon_2(Y_i)$ holds. Varying the sp^2 fraction in a set of samples will cause, through Eqs. (15) and (16), a variation of the $\varepsilon_2(Y_i) \approx \varepsilon_{2\pi}(Y_i)$ value, and a similar variation of the

$\varepsilon_{1\pi}(Y_i)$ value. Moreover, a small variation within W_i values of different samples, will provide only a small spread of experimental data about the foreseen trend. Finally, the intercept $I(Y_i)=\varepsilon_{1\sigma}(Y_i)$ is a slowly increasing function of energy,[10,11] which, in a first order approximation, does not directly depend upon n_π (or, equivalently, on the sp^2 fraction). In summary, a linear relationship

$$\varepsilon_i(Y_i)=I(Y_i)+S(Y_i)\varepsilon_2(Y_i), \tag{17}$$

will be anticipated under the following conditions:

(i) If the relationship is analyzed at a fixed value of Y_i and not at constant photon energy.

(ii) If the contribution of transitions other than π-π^* is negligible in the energy region of interest.

The slope

As mentioned above, an analytical evaluation of the slope is not achievable in the framework of the Gaussian-DOS model, because of the peculiar form of Eq. (6). However, an integration of Eq. (2a) in analytical form can be obtained[12] in the framework of the Gaussian-ν model, by setting the lower limit of the integral arising from KK relation to $-\infty$. With such an additional approximation, we obtain

$$\begin{aligned}\varepsilon_{1\pi}(Y_\nu)-1 &\approx \frac{B}{\pi\sigma'_\pi}\int_{-\infty}^{+\infty}\frac{\exp[-(W_\nu-Y')^2]}{Y'^2-Y_\nu^2}dY' \\ &= \frac{B}{E}\{i\,\mathrm{erf}[i(Y_\nu-W_\nu)]\exp[-(Y_\nu-W_\nu)^2] \\ &\quad + i\,\mathrm{erf}[i(Y_\nu+W_\nu)]\exp[-(Y_\nu+W_\nu)^2]\}.\end{aligned} \tag{18}$$

Dividing by $\varepsilon_{2\pi}(Y_\nu)$ [see Eqs. (12) and (16)] the following B-independent expression for the slope of the $\varepsilon_1(Y_\nu)$ vs $\varepsilon_2(Y_\nu)$ line is found

$$\begin{aligned}S(Y_\nu) &= i\{\mathrm{erf}[i(Y_\nu-W_\nu)] \\ &\quad + \exp(-4W_\nu Y_\nu)\mathrm{erf}[i(Y_\nu+W_\nu)]\} \\ &= i\left\{\mathrm{erf}\left(i\frac{E-P_\pi}{2\sigma'_\pi}\right)\right. \\ &\quad \left. + \exp\left(-\frac{EP_\pi}{\sigma'^2_\pi}\right)\mathrm{erf}\left(i\frac{E+P_\pi}{2\sigma'_\pi}\right)\right\}.\end{aligned} \tag{19}$$

Since Eq. (19) has been demonstrated in the framework of the Gaussian-ν model, a simplification of the Gaussian-DOS one, before moving to the analysis of experimental data, we wish to extimate the error introduced by using the Gaussian-ν model instead of the Gaussian-DOS one. At this purpose we have performed, by varying E_π and σ_π values, a large number of numerical simulations of the type reported in Fig. 8, where the slopes extracted by numerical integrations in the framework of the Gaussian-DOS model are compared to those obtained from Eq. (19) for the Gaussian-ν model. As shown in Fig. 6, differences can be found only for small values of $W_G=E_\pi/\sigma_\pi$, such as those found in sp^2 richest samples.[13]

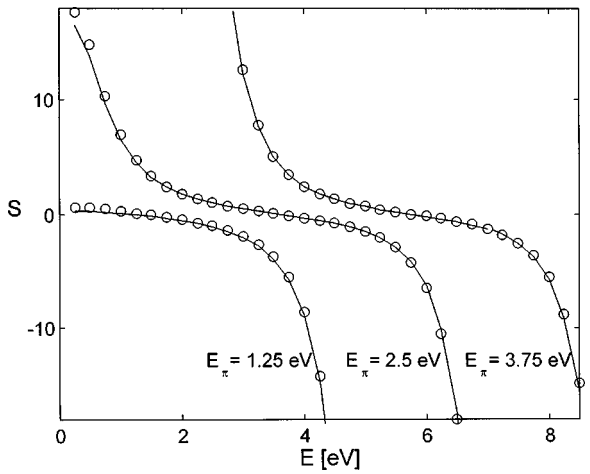

FIG. 6. The comparison between numerical solutions (○) of Gaussian DOS model and the analytical Eq. (12) (—) is performed even for E_π values exaggeratively larger and well lower than the current ones and a constant width $\sigma_\pi=0.875$ eV.

We can conclude that, apart for some very special cases, the Gaussian-ν model is able to give the same amount of information achievable with the more refined Gaussian-DOS model.

The intercept

Eq. (15a) clearly shows that the $\varepsilon_1(Y_i)$ vs $\varepsilon_2(Y_i)$ relationship is not only characterized by the $S(Y_i,W_i)$ value, but it is also affected by the energy dependence of the term $\varepsilon_{1\sigma}(Y_i)$. Since we have shown that, in the energy region of interest in the present work, the transitions of other types than the π-π^* ones give a negligible contribution to the ε_2 trend, it can be argued that $\varepsilon_{1\sigma}(Y_i)$ is independent of the density of π states and, hence, on the slope of the $\varepsilon_1(Y_i)$ vs $\varepsilon_2(Y_i)$ function.

Most of the electronic transitions in amorphous carbons (except π-π^*) will have an onset at photon energies higher (or even much higher) than 4.5 eV. This suggested[10] to treat them as arising from two δ-shaped bands at an interband distance E_0 much higher than the energy range of interest [Wemple-Didomenico (WD) model[11]]. In the framework of such model, a very simple expression for $\varepsilon_{1\sigma}(E)$ can be determined:

$$\frac{1}{\varepsilon_{1\sigma}(E)-1}=\frac{E_0}{E_d}-\frac{1}{E_0E_d}E^2, \tag{20}$$

where E_d is a dispersion energy connected to the amplitude of σ states related transitions (σ-π^*, etc.). Since dimensionless variables Y_i have been used in the evaluation of the slope, we will use the same dimensionless variables for analyzing the intercept, rewriting Eq. (20) as follows:

$$I(Y_i)=\varepsilon_{1\sigma}(Y_i)=1+\frac{1}{X_0-X_iY_i^2}, \tag{21}$$

where $i=G$ or ν and

$$X_0=\frac{E_0}{E_d},\quad X_G=\frac{4\sigma_\pi^2}{E_0E_d},\quad X_\nu=\frac{4\sigma'^2_\pi}{E_0E_d}. \tag{22}$$

THE *n* VS *k* RELATIONSHIP

From Eqs. (3) and (17), we can work out a relationship between the refractive index n and the extinction coefficient k at a given Y_i value ($i=G$ or ν):

$$n(Y_i)=S(W_i,Y_i)k(Y_i) + \sqrt{[S(W_i,Y_i)^2+1]k(Y_i)^2+I(X_0,X_i,Y_i)}. \tag{23}$$

Actually, the presence of the square-root term on the left-hand side of Eq. (23), renders the relationship between n and k not strictly linear, but its departure from linearity is low (at least when a set of samples with a low excursion of $k(Y_i)$ is considered). If such approximation holds, we can rewrite Eq. (23) for low-k values as

$$n(Y_i)\approx S(W_i,Y)k(Y_i)+\sqrt{I(X_0,X_i,Y_i)}, \tag{24}$$

where the slope is almost the same of the corresponding ε_1 vs ε_2 one (at the same Y_i value) and the intercepts of the two lines are in a square-root relationship.

EFFECTS OF THE HYPOTHESIS

In this paragraph the most restrictive hypotheses made in the model are considered and their effect on the resulting behavior of the n vs k curve is examined.

(a) *E_π/σ_π ratio nondependent on sp^2 content*. Due to the effect of distortions, stress, and mechanical interference between sp^2 clusters, the values of E_π and σ_π will be in some way correlated to the sp^2 content. However, previous analyses[6,10] have shown that the range of variation of their ratio is narrow, unless the sp^2 fraction exceeds 0.7 in almost unhydrogenated films.[13]

(b) *$\varepsilon_{1\sigma}(E)$ nondependent on sp^3 content*. Since each sp^2-coordinated carbon atom contributes 3 σ states and each sp^3 coordinated contributes 4, it is obvious that the density and distribution of σ states varies from one sample to another. This will reflect in the $\varepsilon_{1\sigma}(E)$ shape and intensity. In turn, this will lead to a variation of $\varepsilon_{1\sigma}(E)$ with sp^2 fraction. However, since the variations in $\varepsilon_{2\sigma}(E)$ occur at much higher energies than those of interest and, moreover, are averaged by a factor $(E^2-E'^2)^{-1}$, their effect is clearly a second-order one of limited importance.

(c) *n_π dependent only on sp^2 fraction*. Actually, it depends upon density too. It is true that density is consequent to the sp^2 fraction and the local structure, but surely not in such a simple way as represented in Eq. (8). This effect, however, is not of great importance, since the densities of the films do not vary more than 10–15%.

(d) *Lower integration limit moved to $-\infty$ in* Eq. (11). The effect of this approximation is negligible as far as the condition $W_\nu>1$ is fulfilled. In such condition, the Gaussian curve will have a negligible tail at negative Y_ν, so that the moving of the lower integration limit from 0 to $-\infty$ has no influence on the result.

The fact that the hypotheses are almost, but not completely, fulfilled, will explain the wide scatter of data around the interpolating line derived from Eq. (17).

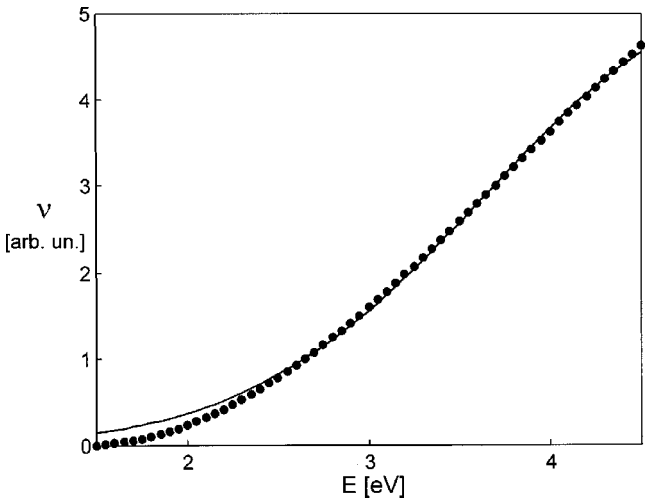

FIG. 7. Experimental data (○) and Gaussian-ν model best fit (—) for sample $C7$.

ANALYSIS OF EXPERIMENTAL DATA

The quality of the fit of ε_2 obtained by using the Gaussian-ν model can be observed in Fig. 7. It is reasonably good at least at not too low photon energies (not too close to Fermi level). In Table II the best fit values for both models (Gaussian-DOS and Gaussian-ν) are reported together with the E_{04} values for all samples considered in the present paper. Only samples $C2$ and, especially, $C1$ show much lower E_{04} values, indicating[9] a much larger amount of sp^2 sites, probably above the percolation threshold. In such cases the Gaussian-DOS model is known to need a modification, due to the interaction of the contiguous sp^2 clusters.[13] In fact, we would like to point out that the results achievable by applying the Gaussian-DOS model[6,14] can be summarized as follows.

(a) In sp^3-rich samples, either hydrogenated or not, the model fits properly the ε_2 spectra up to about 5 eV although the fits does not work properly at low energies (below 2.5 eV).

(b) In sp^2-rich samples, either hydrogenated or not, the models fail to reproduce the overall trend, while it properly fits the low ($<$2.5 eV) energy region.

In case (a) the Gaussians describe the main contribution to the π-DOS, while in case (b) they describe simply the π-DOS close to Fermi level. Then, care has to be taken when the results obtained for group (a) films are compared with those obtained for type (b) films.

In the present case, the Gaussian model is found to be appropriate for films $C2$-$C9$ and, in the lower part of Y_ν spectrum, for film $C1$ [a type (b) film] too. The departure of sample $C1$ from the linear $\varepsilon_1(Y_\nu)$ vs $\varepsilon_2(Y_\nu)$ relationship gradually appears for scaled energies $Y_\nu \geqslant 1.2$ (i.e., $E \geqslant 2.5$ eV) and could be related to the possible presence of the percolation threshold in that DOS region of the quoted sample.

Figure 8 shows the experimental slopes of the ε_1 vs ε_2 lines at all Y_ν values, together with the best fit obtained by using Eq. (19) and the value $W_\nu=2.39$ for the scaled peak energy. This W_ν value should be compared with the values given in Table II. Note that W_ν represents the ratio of the peak energy to the peak width, so that the model performs

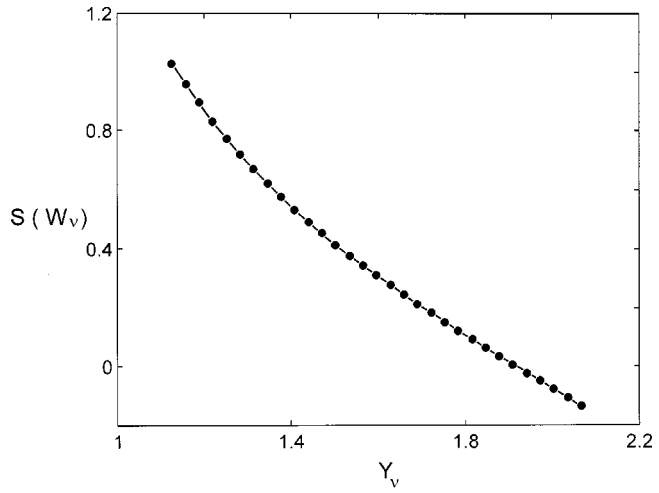

FIG. 8. Experimental data (●) for the slope of the $\varepsilon_1(E)$ vs $\varepsilon_2(E)$ lines and best fit (—) obtained using Eq. (19) and $W_\nu = 2.391$.

well at least when films whose π bands are narrow enough to have a negligible tail near Fermi level are considered. Figure 9 shows, in a WD plot, that a good agreement is obtained between the experimental values and the WD curve for which the values of $X_0 = 0.421$ and $X_\nu = 0.013$ are used for the dimensionless parameters of Eq. (21). Using for σ'_π its average value 0.96 eV (from Table II), we obtain $E_0 = 11.2$ eV and $E_d = 26.5$ eV. If we compare such values with those typically found for a-Si:H ($E_0 = 2.2-2.6$ eV and $E_d = 30-40$ eV[15]); we observe that the E_0 value reasonably scales like the σ-σ^* states energy gap (compare for instance diamond 5.5 eV gap and c-Si 1.11 eV gap). As E_d is concerned, being its value proportional to the volume density of valence electron,[15] we would have expected in fact the a-Si:H value to be larger, since in the a-C(:H) case π states do not give their contribution to E_d (see above).

Going back to Fig. 9, where the typical dispersive behavior far from resonance's of $\varepsilon_{1\sigma}$ is evident, it should be noted that an incorrect normalization of energy scale (for instance using E instead of Y_ν) will markedly distort the trend of $I(Y_\nu)$, as can be seen by comparing Figs. 5 and 9. The role played by the σ_π scaling becomes crucial: in order to understand the meaning of such a role, it is important to remember the large impact that disorder has in determining the width of Gaussian bands. By operating the σ_π scaling, then, it is possible to take into account the different amount of disorder in different samples. This allows a comparison between optical properties in regions where the effect of disorder is similar. In contrast, a comparison made at a given photon energy E (without σ_π scaling) will disregard such an effect and mix up the real behaviors.

CONCLUSION

In this paper it is reported that, as far as thin films of hydrogenated (and not hydrogenated) amorphous carbon are considered, a linear relationship exists between the real and imaginary parts of the dielectric constant for energies in the range 1.5–4.5 eV. We have shown that such a behavior can be foreseen in the framework of the Gaussian-DOS model

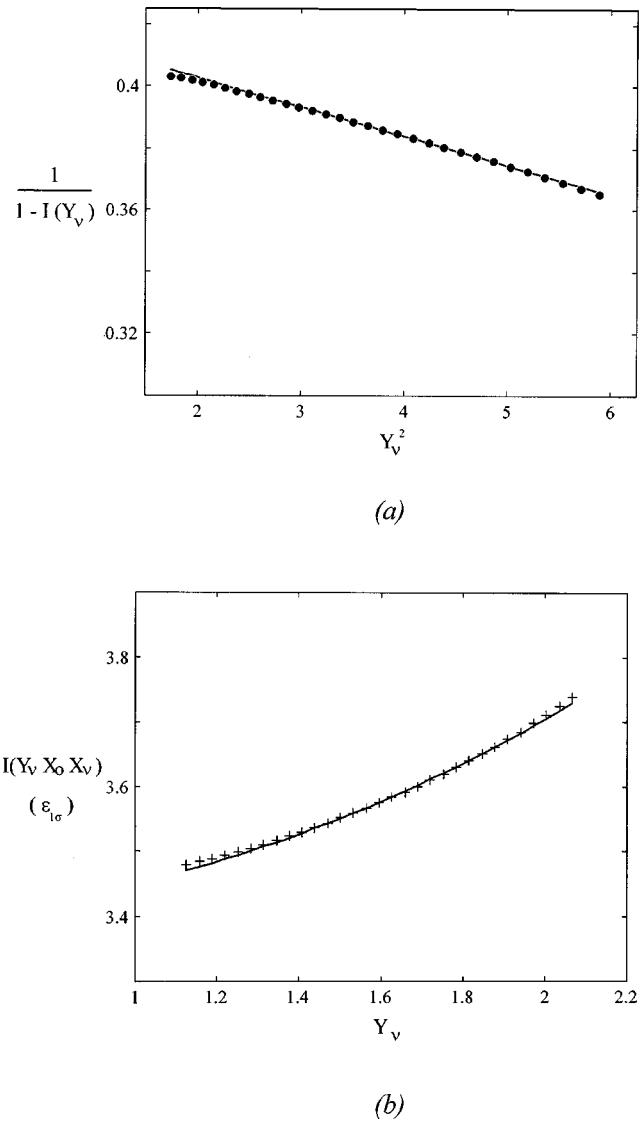

FIG. 9. (a) Wemple-Didomenico plot and (b) $I(=\varepsilon_{1\sigma})$ behavior vs normalized energy Y_ν with appropriate best fits obtained by Eq. (21) employing $X_0 = 0.421$ and $X_\nu = 0.013$.

for the π states,[6] once the difference among the band width in different samples is taken into account through a normalization of the energy scale, achieved by introducing the scaled energy $Y = E/(2\sigma_\pi)$. As said above, this can be interpreted in the light of the role that the local disorder assumes in determining the σ_π value. The Gaussian-DOS model itself is able to properly reproduce the energy dependence of the intercept and slope of the linear interpolation of ε_1 vs ε_2 and n vs k. However, through the Gaussian-DOS model approximation to the Gaussian-ν model (where a Gaussian shape is assumed directly for $E\varepsilon_2$), an analytical expression of the Y dependence for the slope of the linear interpolation of ε_1 vs ε_2 and n vs k has been evaluated. In summary, the origin of such a linear behavior can be found in the peculiar Gaussian form of the DOS bands (the π and π^* ones) involved in the optical transitions.

It has also been shown that the intercept value can be interpreted in the framework of the Wemple-Didomenico model as due to contribution to ε_1 of the transitions involving the σ states and occurring far from the energy region of interest in the optical analysis.

[1] A. Bubenzer, B. Dischler, G. Brandt, and P. Koidl, J. Appl. Phys. **54**, 4590 (1983).
[2] J. Robertson, Adv. Phys. **35**, 317 (1986).
[3] G. Cody, in *Semiconductors and Semimetals*, edited by J. Pankove (Academic, New York, 1984), Vol. 21.
[4] D. P. Dowling, K. Donnelly, M. Monclus, and M. McGuinness, Diamond Relat. Mater. **7**, 432 (1998).
[5] K. Donnelly, D. P. Dowling, T. P. O'Brien, A. O'Leary, and T. C. Kelly, Diamond Relat. Mater. **5**, 445 (1996).
[6] D. Dasgupta, F. Demichelis, C. F. Pirri, and A. Tagliaferro, Phys. Rev. B **43**, 2131 (1991).
[7] D. P. Dowling, P. V. Kola, K. Donnelly, T. C. Kelly, K. Brumitt, L. Lloyd, R. Eloy, M. Therin, and N. Weill, Diamond Relat. Mater. **6**, 390 (1997).
[8] D. Y. Smith, in *Handbook of Optical Constants of Solids*, edited by E. Palik (Academic, New York, 1985).
[9] J. Robertson, Philos. Mag. B **76**, 335 (1997).
[10] F. Demichelis, C. F. Pirri, and A. Tagliaferro, Phys. Rev. B **45**, 14 364 (1991).
[11] S. H. Wemple and M. Didomenico, Phys. Rev. B **3**, 1338 (1971).
[12] *Handbook of Mathematical Functions*, edited by M. Abramowitz and I. Stegun (Dover, New York, 1965).
[13] S. Neuville and A. Tagliaferro (unpublished).
[14] V. Paret, Ph.D. thesis, Université Pierre et Marie Curie, Paris, 1999.
[15] F. Demichelis, E. Minetti-Mezzetti, A. Tagliaferro, E. Tresso, P. Rava, and N. M. Ravindra, J. Appl. Phys. **59**, 611 (1986).